Data, Innovation, and Science Cluster

Validation report (TN-04)

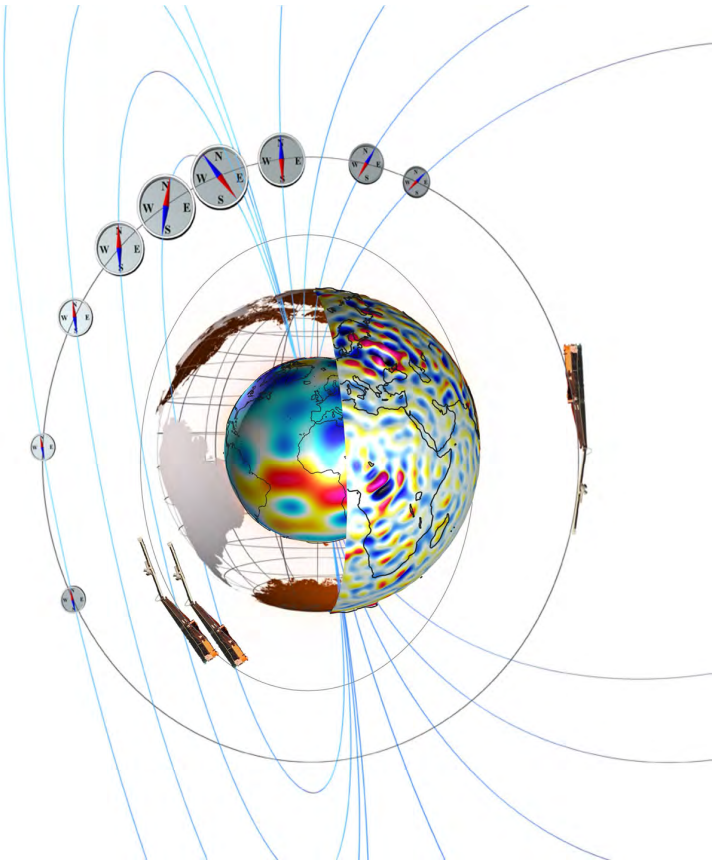

Doc.No: SW-TN-OULU-SWIPE_01, Rev: 2

Prepared:	Prepared:
Heikki Vanhamäki Work package manager Date 08–02–2024	Habtamu Tesfaw Project Scientist Date 08–02–2024
Approved:	Checked:
Spencer Hatch Project Manager Date 08–02–2024	??? ??? Date 08–02–2024

Record of changes

Reason	Description	Rev	Date
Issue 1	Draft	1	04-12-2023
Issue 2	Revised	2	31-01-2024

Table of Contents

Preface

This document describes validation of the Swarm High-latitude Convection (Swarm Hi-C) model developed in the Swarm Ionospheric Polar Electrodynamics (SWIPE) project. The manuscript Hatch et al. [2023] presents several examples of the electric potential, electromagnetic work and the Hall and Pedersen conductances produced by the Hi-C model, including comparisons of the cross polar cap potential (CPCP) with other relevant models. This report expands the validation effort by presenting some synthetic test cases and by presenting comparisons to the statistical models and simulations used in the storm of 14-16 December 2006 that was part of the GEM-CEDAR challenge [Rastätter et al., 2016]. In addition, the Pedersen conductance produced by the Hi-C model is compared with those calculated from the same Swarm dataset using the method by Sugiura et al. [1982].

1 Synthetic examples

To give an overview of the output and general behavior of the Swarm Hi-C model, in addition to the examples provided by Hatch et al. [2023], we first present some synthetic examples where either the IMF B_z component or the solar wind speed is varied, while all the other input parameters have constant values. Figures 1 and 2 show the model output for the northern and southern hemispheres (NH and SH), respectively, in a case where the IMF B_z gets values -5, -2, 2 or 5 nT. Different values of IMF B_z correspond to different columns, while the electrostatic potential, electromagnetic work and the Hall and Pedersen conductances given by Hi-C are at different rows. The other input variables have the constant values of V = 400 km/s, B_y = 0 nT, dipole tilt = 0°, F10.7 = 120. In plotting the electromagnetic work and the conductances, the unreliable or

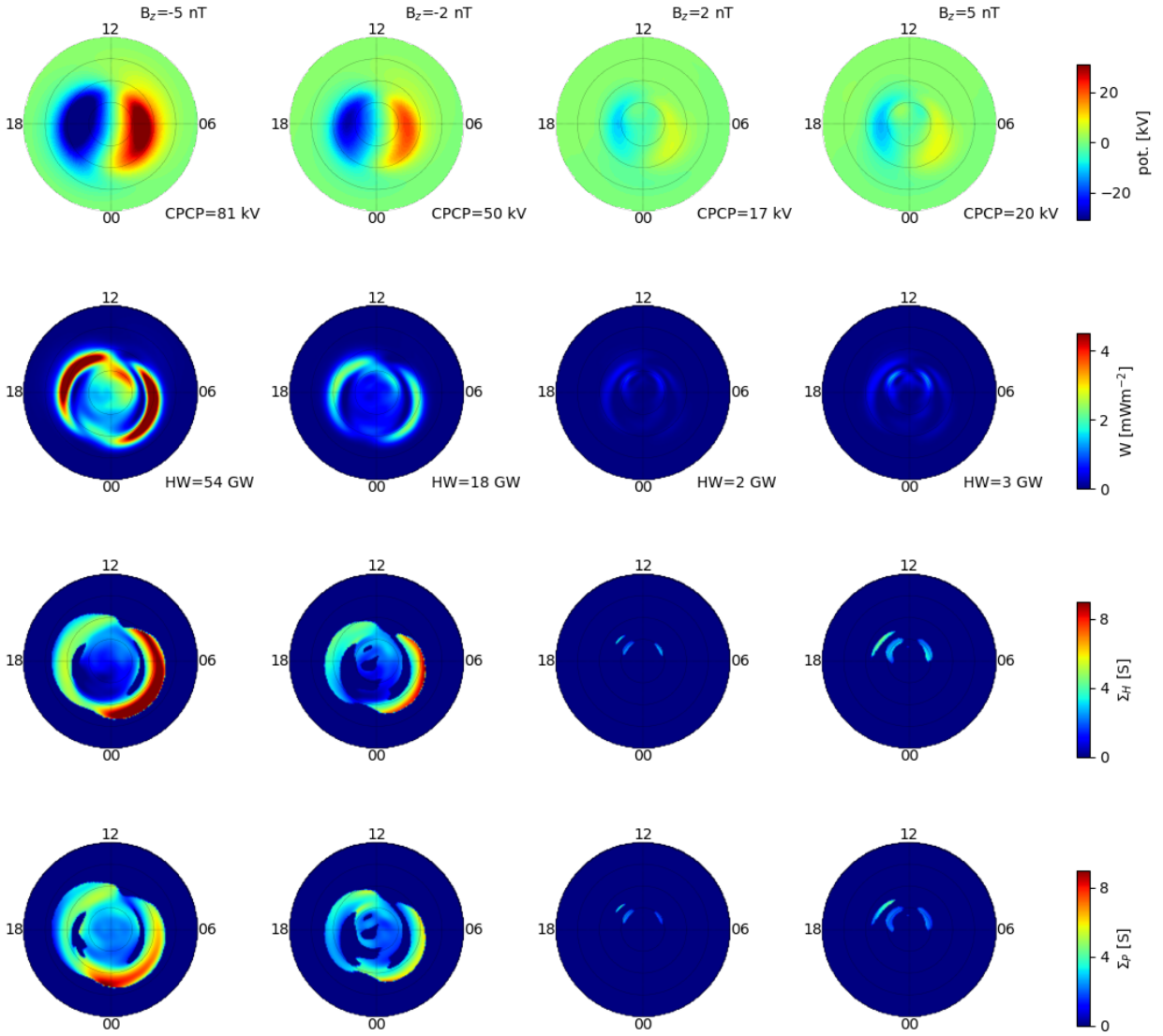

Figure 1: Effect of IMF B_z on Hi-C model in the NH. Columns: B_z = -5, -2, 2 and 5 nT. Rows: electrostatic potential, electromagnetic work, Hall conductance and Pedersen conductance. Other input parameters have constant values V = 400 km/s, B_y = 0 nT, tilt = 0°, F10.7 = 120.

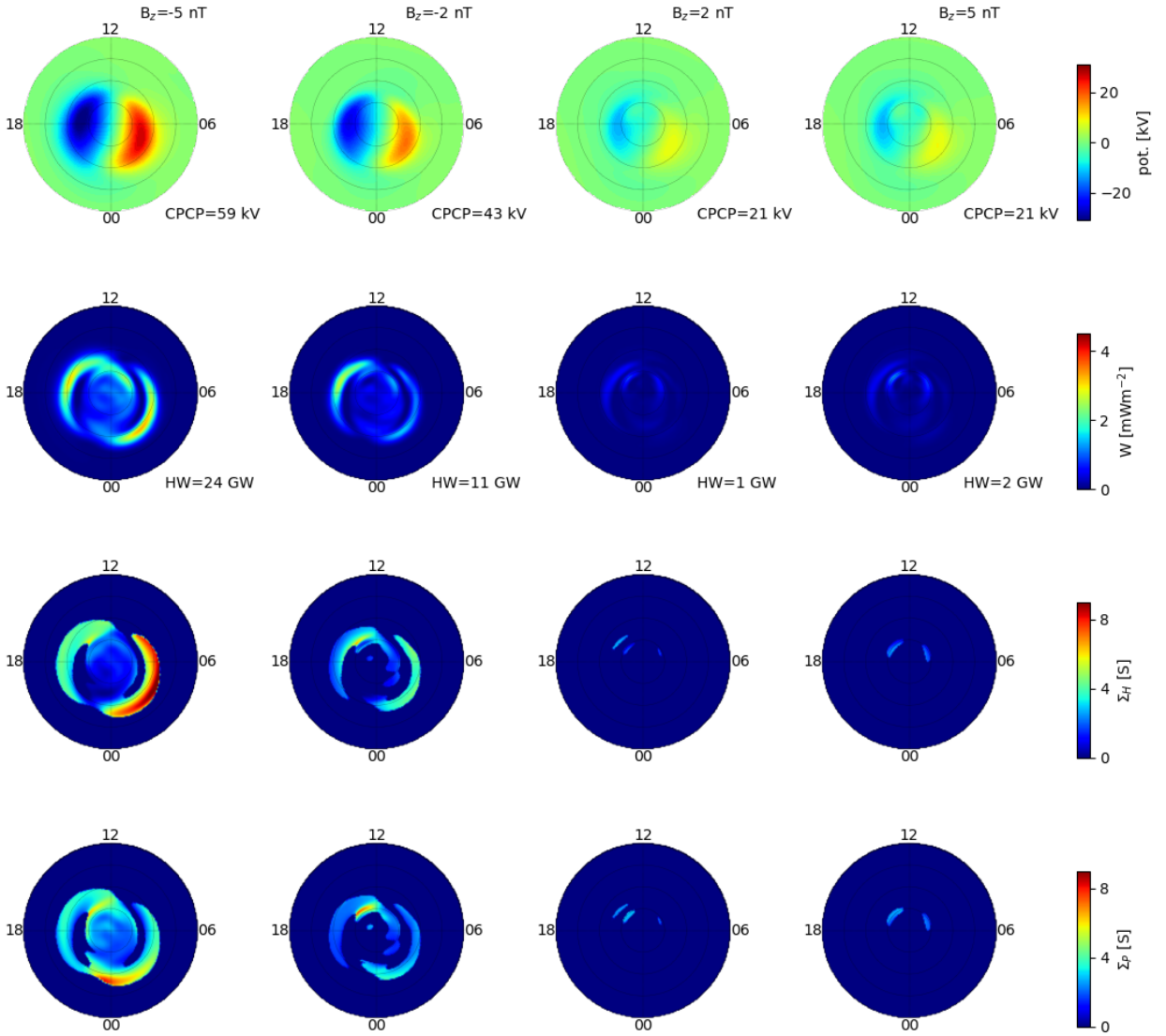

Figure 2: Same as Figure 1, but for the SH.

nonphysical regions have been set to zero using the criteria in Equation 37 of Hatch et al. [2023].

The Hi-C output behaves very much as expected: the most intense convection, the largest electromagnetic work and the largest conductances are seen for IMF $B_z = -5$ nT, with sharply decreasing activity for IMF $B_z = -2$ or 2 nT. There is a small increase in the cross polar cap potential (CPCP) and hemispherically integrated electromagnetic work when the IMF B_z changes from 2 to 5 nT, which indicates that the Hi-C model captures the increase of solar wind energy input via lobe reconnection and viscous interactions that take place during increasingly northward IMF.

Comparison of Figures 1 and 2 shows that the general behaviour in the two hemispheres is the same and also the patterns are very similar. A closer inspection reveals some hemispheric differences, with the NH typically having more intense convection and larger electromagnetic

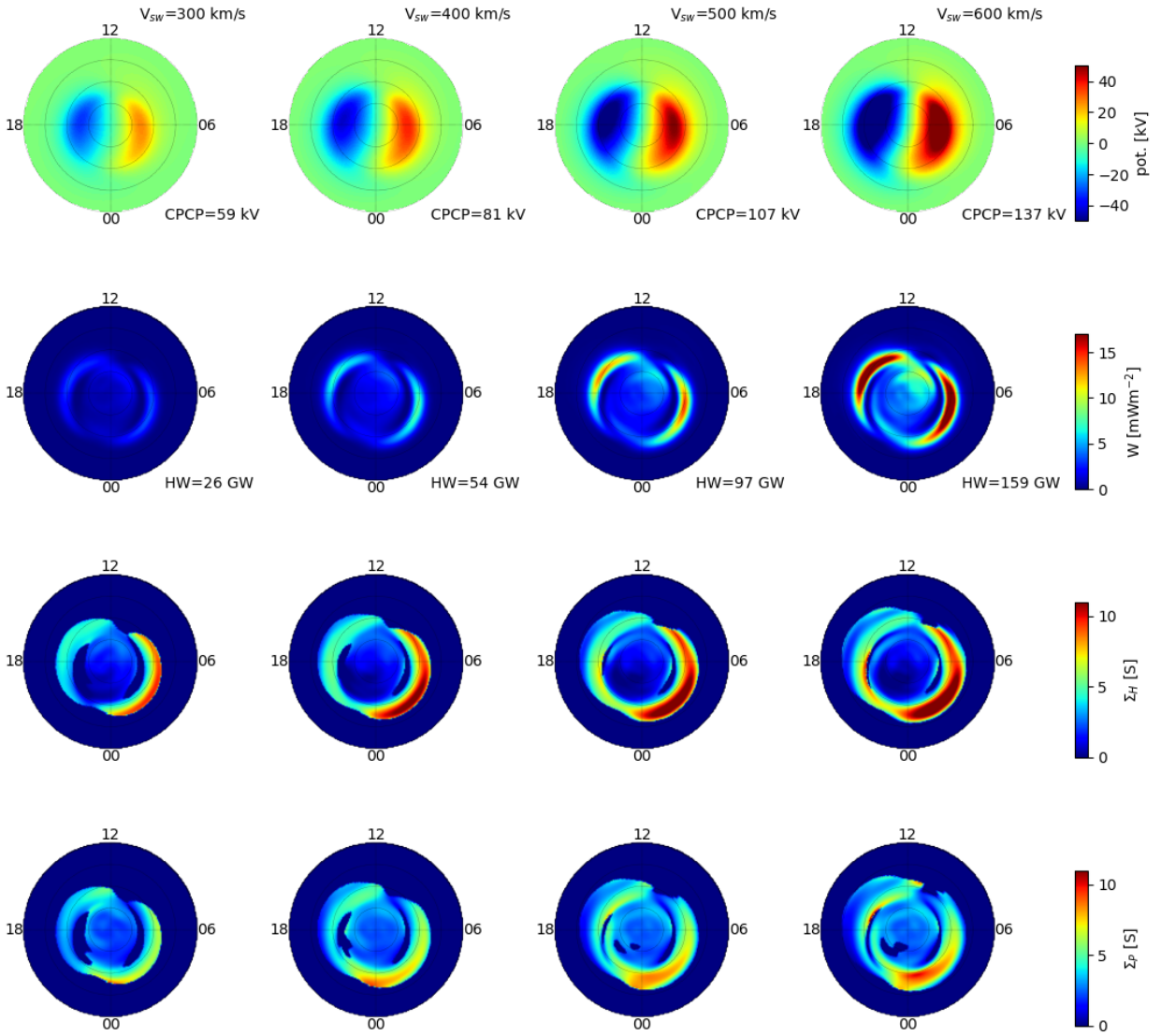

Figure 3: Effect of solar wind speed on Swipe in the NH. Columns: V = 300, 400, 500 and 600 km/s. Rows: potential, electromagnetic work, Hall conductance and Pedersen conductance. Other parameters have constant values B_z = -5 nT, B_y = 0 nT, tilt = 0°, F10.7 = 120.

work. A more detailed hemispheric comparison is given by Hatch et al. [2023], so we do not go into details here.

Figures 3 and 4 show the model output in NH and SH in the same format as the previous figures, but for a case where the solar wind speed gets increasingly large values of 300, 400, 500 and 600 km/s. In this case the other input variables have fixed values of B_z = -5 nT, B_y = 0 nT, tilt = 0°, F10.7 = 120.

Also in this speed variation case we can observe that the Hi-C model behaves in a reasonable and expected manner: convection described by the potential, electromagnetic work and conductances

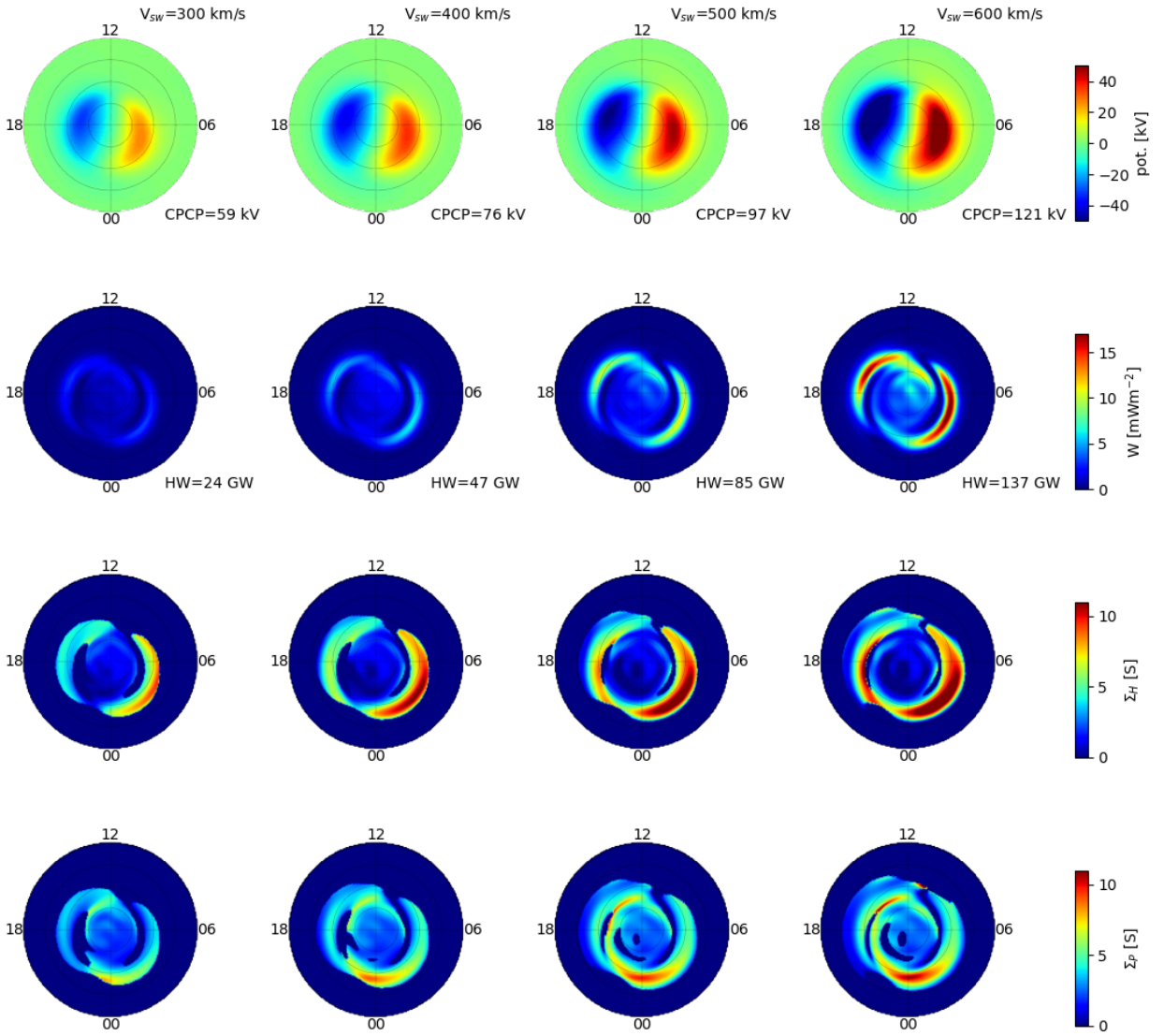

Figure 4: Same as Figure 3, but for the SH.

increase monotonically in both hemispheres as the solar wind speed increases. It can also be seen that the convection cells expand equatorward when the solar wind energy input increases, although movement of the auroral oval (approximated by the electromagnetic work and conductances) is not very clear. A more detailed comparison of the Figures 3 and 4 again reveals some hemispheric differences, with the NH again showing larger CPCP and electromagnetic work. It seems that the hemispheric difference increases with solar wind speed: for 300 km/s both hemispheres have the same CPCP of 59 kV, but for speed of 600 km/s the difference has increased to 16 kV or 12%.

2 GEM-CEDAR challenge

In order to compare the Hi-C model to other statistical models and simulations in a real event, we selected one of the storms used in the GEM-CEDAR challenge, namely the 14-16 December 2006 storm as our test case. The modeling challenge was initiated by the Geospace Environment Modeling (GEM) and the Coupling Energetics and Dynamics of Atmospheric Regions (CEDAR) communities in order to compare models of auroral boundaries and the energy flux from the magnetosphere into the ionosphere. The challenge and the models are described in detail by Rastätter et al. [2016] and the results of the models runs can be accessed via the Community Coordinated Modeling Center at [URL1].

2.1 The storm of 14-16 December 2006

Figure 5 shows the solar wind speed and IMF components together with the SYM-H index for the storm of 14-16 December 2006 selected as our test event. It should be noted that in the figure the speed and IMF are shown as averages of the preceding 20 min, as that is used as input in the Hi-C model. This averaging was chosen to match the procedure used in constructing the Hi-C model, as explained in Hatch et al. [2023]. As the solar wind data is taken from OMNI [URL2], it is already propagated to the bow shock. In contrast, the SYM-H index is plotted without the averaging.

It can be seen that the solar wind conditions during this storm reach extreme values, with the solar wind speed close to 900 km/s for several hours. Also the IMF B_z and B_y components reach magnitudes over 10 nT for prolonged periods. The most intense driving takes place from 14-Dec UT 23 to 15-Dec UT 05 during which period the solar wind speed is high and the IMF B_z is strongly negative. This period also contains the storm's main phase with SYM-H dropping to -211 nT.

In Sections 3-5 we present time series of the CPCP and hemispherically integrated electromagnetic work from Hi-C and other selected models. We have also selected three time instants, representing different activity levels for closer inspection. These times are marked in Figure 5 and summarized in Table 1. For these time instant we show magnetic latitude - magnetic local time (Mlat-MLT) distributions of the potential, electromagnetic work and conductances in Sections 3-5.

Table 1: Summary of the three selected time instants. They are also marked in Figure 5.

	date and UT	Sym-H (nT)	speed (km/s)	IMF B_z (nT)	IMF B_y (nT)
Quiet	14-Dec 12:39	-9	560	-1.7	-0.3
Moderate	15-Dec 17:51	-74	602	-3.7	2.6
Active	14-Dec 23:45	-126	837	-14.6	5.7

Comparing the solar wind values shown in Figure 5 to the distribution of data points shown in Figure 1 of Hatch et al. [2023] used to construct the Hi-C model, it is clear that this test event lies in a part of the parameter space that is poorly sampled by Swarm data. This is especially true for the "active" time step, while the "quiet" time step is somewhat better covered in the model construction. On one hand this means that we are not testing the most typical solar wind conditions, and therefore our results and conclusions may not be totally general. On the other hand, the most extreme events are often the most interesting both in terms of science and space

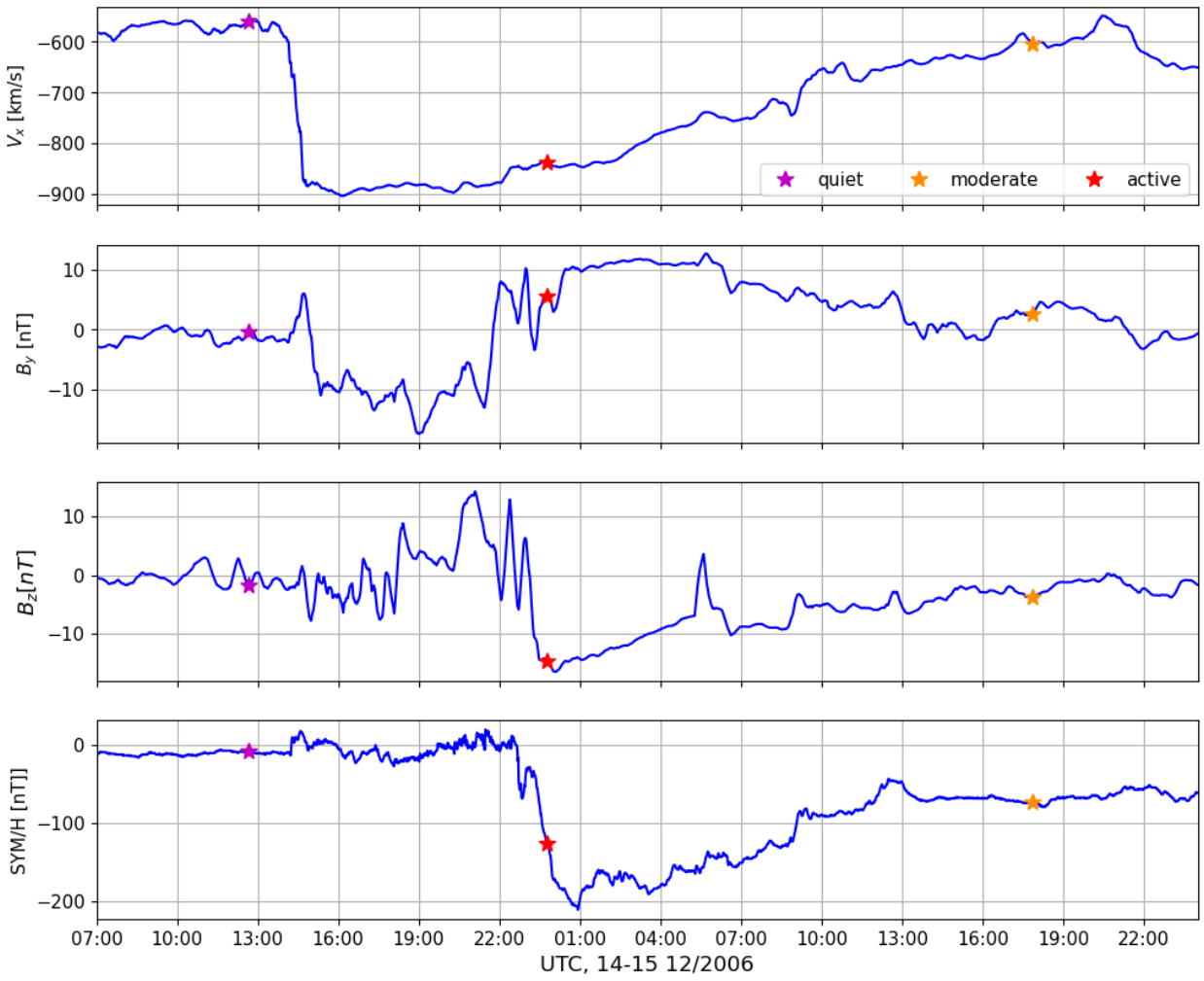

Figure 5: The Solar wind driving (the first three panels) and the SYM-H index (the last panel) during the GEM-CEDAR storm. The stars mark three selected time instants, quiet (14 Dec 12:39, violet), moderate (15 Dec 17:51, orange) and active (14 Dec 23:45, red) which are used for detailed comparison of the selected models in Sections 3-5. The solar wind parameters are averaged over 20 minutes preceding a given time instant.

weather applications. At the same time we push the model into extreme domain, which may reveal behaviour that would not be apparent in more typical conditions.

2.2 Simulations at CCMC and other models

Table 2 shows a summary of the simulations and statistical models used in the following Sections. The first five models, i.e. the statistical Weimer model and all the simulations, are taken from the GEM-CEDAR challenge database at CCMC. The last two models, i.e. the SuperDARN convection model by Thomas and Shepherd [2018] and the conductance model by Hardy et al. [1987] have been added to the comparisons using the codes available at NASA CCMC's Instant Run System and the Lompe GitHub repository, respectively.

Table 2: Summary of the selected models available at CCMC (top part) and other models used in the comparisons (bottom part). The table shows inputs and outputs that are relevant to our study. The data output of the CCMC model runs can be accessed from the web pages mentioned in the last column of the table.

model	type	input	output	reference
Weimer	statistical	Solar wind speed, density, IMF B_y and B_z and dipole tilt angle	electric potential and Joule heating	Weimer [2005]; [URL4]
OpenCGM	MHD simulation	Solar wind and IMF parameters	electric potential, FAC, Hall and Pedersen conductances	URL5
SWMF	combination of various magnetospheric and ionospheric models	Solar wind density , velocity, temperature and the IMF	electric potential, FAC, Hall and Pedersen conductances	URL3
LFM-MIX	MHD simulation	Solar wind speed, density, the IMF, dipole tilt angle	electric potential, current, Joule heating, conductance, etc	URL6
CMIT	coupling of the LFM-MIX model with the TIE-GCM thermosphere-ionosphere model	LFM-MIX inputs, solar EUV and F10.7 index	electric potential, current, Joule heating, conductance, etc	URL7
TS18	statistical	Solar wind speed, IMF B_y and B_z, and dipole tilt angle	Electric potential and ionospheric convection velocity	Thomas and Shepherd [2018]
Hardy	statistical	Kp index	Hall and Pedersen conductances	Hardy et al. [1987]
Cosgrove-PF	Statistical	Solar wind density, velocity, and the IMF	Poynting Flux	Cosgrove et al. [2014]

3 Potential and CPCP

In this section we compare the electrostatic potential and CPCP produced by Hi-C (or SWIPE) model to the other models listed in Section 2.2 in the storm event described in Section 2.1.

Figure 6 presents the Mlat-MLT distributions of the electrostatic potential in the NH (upper part) and SH (lower par) for the moderate activity case from Hi-C (SWIPE) and the models available at CCMC (listed in Table 2). It can be seen that the two statistical models, SWIPE and Weimer, are very close to each other, while the simulations show large differences both between themselves and to the statistical models. Apart from the LFM-Mix model, the CPCP values are in the same ballpark.

In Figure 6 the differences between the NH and SH are larger than exhibited by SWIPE in the synthetic cases presented in Section 1 or in the article Hatch et al. [2023]. This is understandable, since the storm takes place close to the winter solstice in the NH and during the selected time instant the IMF B_y is positive.

For a better comparison between statistical models, Figure 7 shows the electrostatic potentials at NH (top row) and SH (bottom row) from the SWIPE, Weimer and TS18 models. It can be noted that the SWIPE and Weimer models are more similar to each other than to the TS18 based on SuperDARN data.

Figure 8 shows a comparison between selected models, namely SWIPE, Weimer and SWMF for the three activity levels described in Section 2.1. It can be seen that the simulation is significantly different from the two statistical models even in the quiet conditions, although it should be remembered that even in the quiet case the solar wind speed is quite large. At moderate and active conditions SWMF does reproduce the expected two-cell patter, but the morning cell is exceedingly weak compared both to the evening cell and to the statistical models.

It is noteworthy that in Figure 8 the CPCP and general strength of the convection produced by the SWIPE model increases markedly from the moderate to active conditions. In contrast, the Weimer and SWMF models show a much smaller increase, possibly indicating some type of saturation of the CPCP in response to extreme solar wind driving. From the parametrization of the SWIPE model given in Equations 21–22 of Hatch et al. [2023] it should be expected that SWIPE reacts almost linearly to extreme driving, without any saturation. Another notable point is the latitudinal extent of the convection cells in the SWIPE and Weimer models during the active conditions. Also this difference should be the result of the different parametrizations used in these statistical models.

Finally, Figure 9 presents time series of the CPCP in the northern (top) and southern (bottom) hemispheres during the whole storm. Also the Newell coupling function ϵ [Newell et al., 2007] is included in the plot, with a separate scale on the right side. It is very clear that in both hemispheres the SWIPE and LFM-Mix models reach the highest CPCP values and their time series correlates very well with ϵ with almost linear scaling.

In order to display the CPCP time series more clearly, Figure 10 shows only the SWIPE, Weimer and LFM-Mix models, while adding the CPCP from the SuperDARN gridded data product [URL8]. It is clear that in the beginning and end of the time series, when the solar wind conditions are

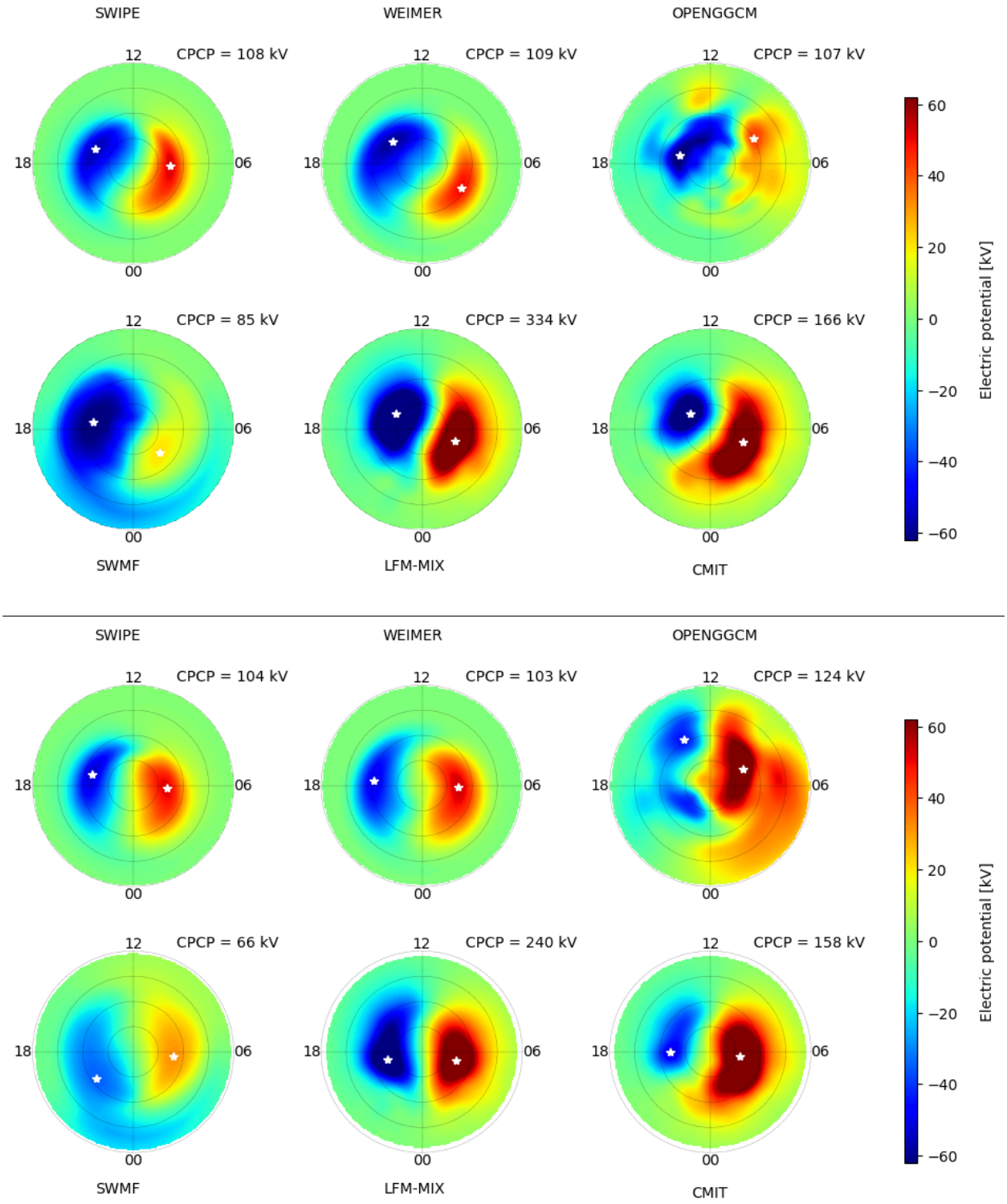

Figure 6: Electric potential from SWIPE and models from CCMC for the moderate conditions described in Figure 5 and Table 1. NH at top, SH at bottom. White stars mark the potential minimum and maximum locations.

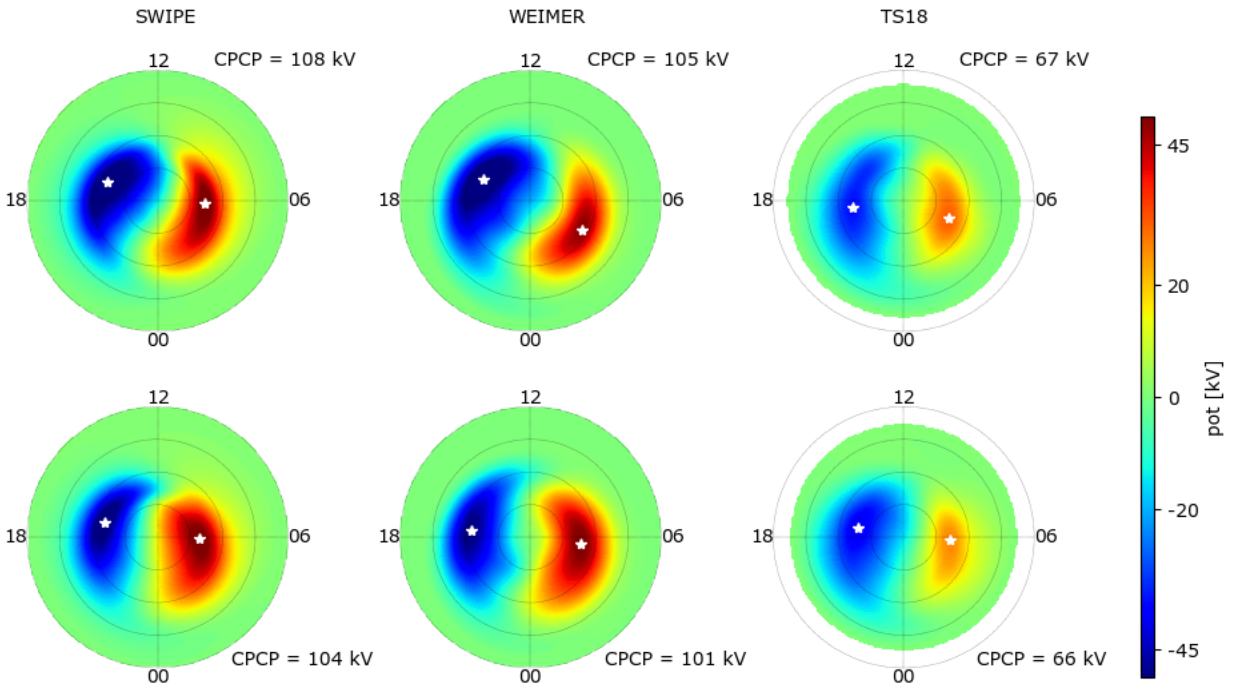

Figure 7: Potential from the three statistical models SWIPE, Weimer-05 and TS18 or the moderate conditions described in Figure 5 and Table 1. Top row NH, bottom row SH.

reasonably normal according to Figure 5, the SWIPE and Weimer models are very similar and the curves overlap in many places. However, under the extreme solar wind conditions during the storm's main phase, the SWIPE model deviates from the Weimer model and follows more closely the LFM-Mix simulation. In contrast, the CPCP from the SuperDARN gridded data product shows much smaller values during the storm. It should be noted that this event took place in 2006, when there were no mid-latitude SuperDARN radars. Thomas and Shepherd [2018] show that without the mid-latitude radars the CPCP can be severely underestimates during active conditions.

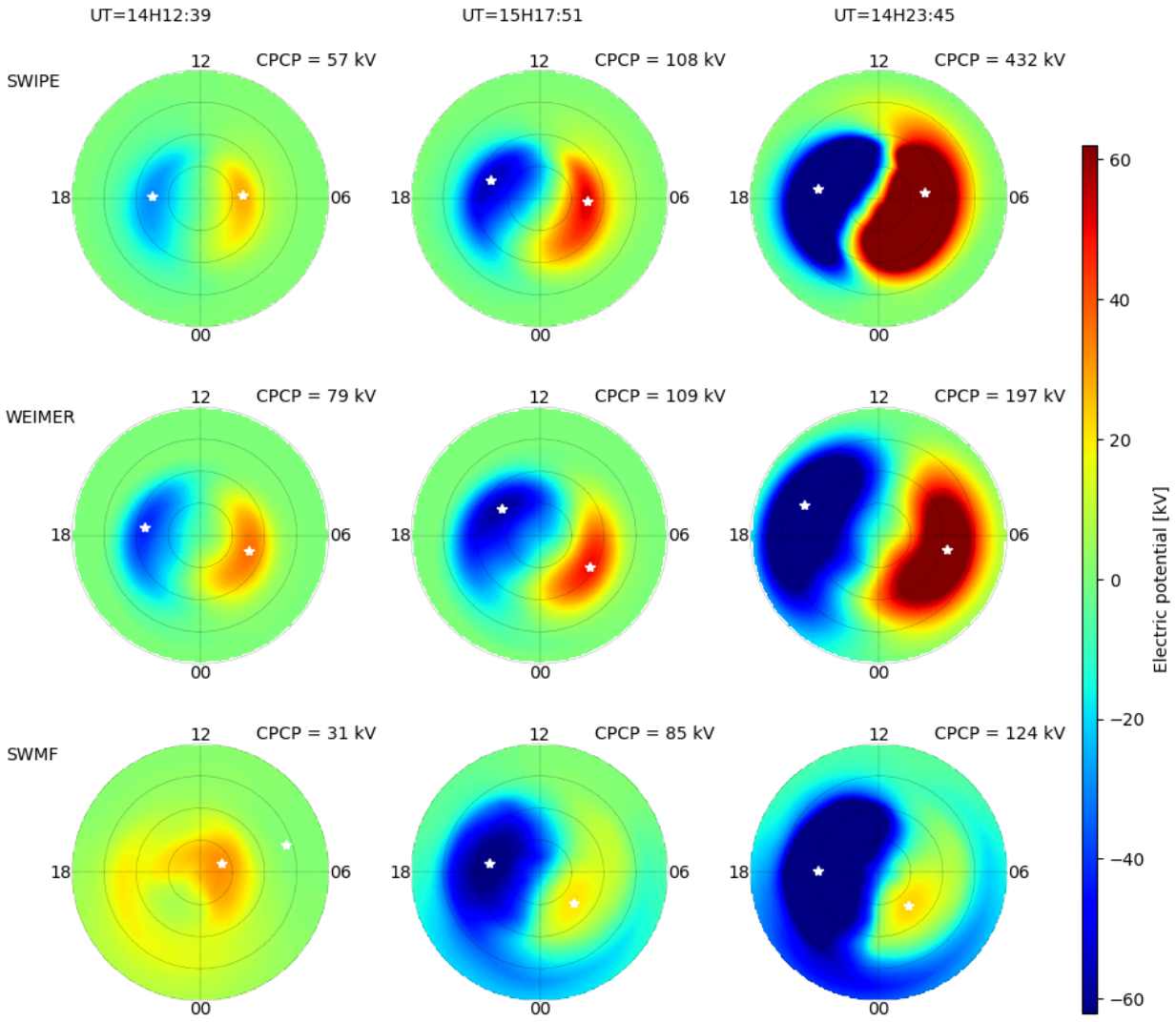

Figure 8: Potential at NH from SWIPE (top row), Weimer-05 (middle row) and SWMF (bottom row) at the three selected times indicated in Figure: left 15-Dec 21:07 UT (quiet conditions), middle 14-Dec 14:50 UT (moderate) and right 14-Dec 23:45 UT (active).

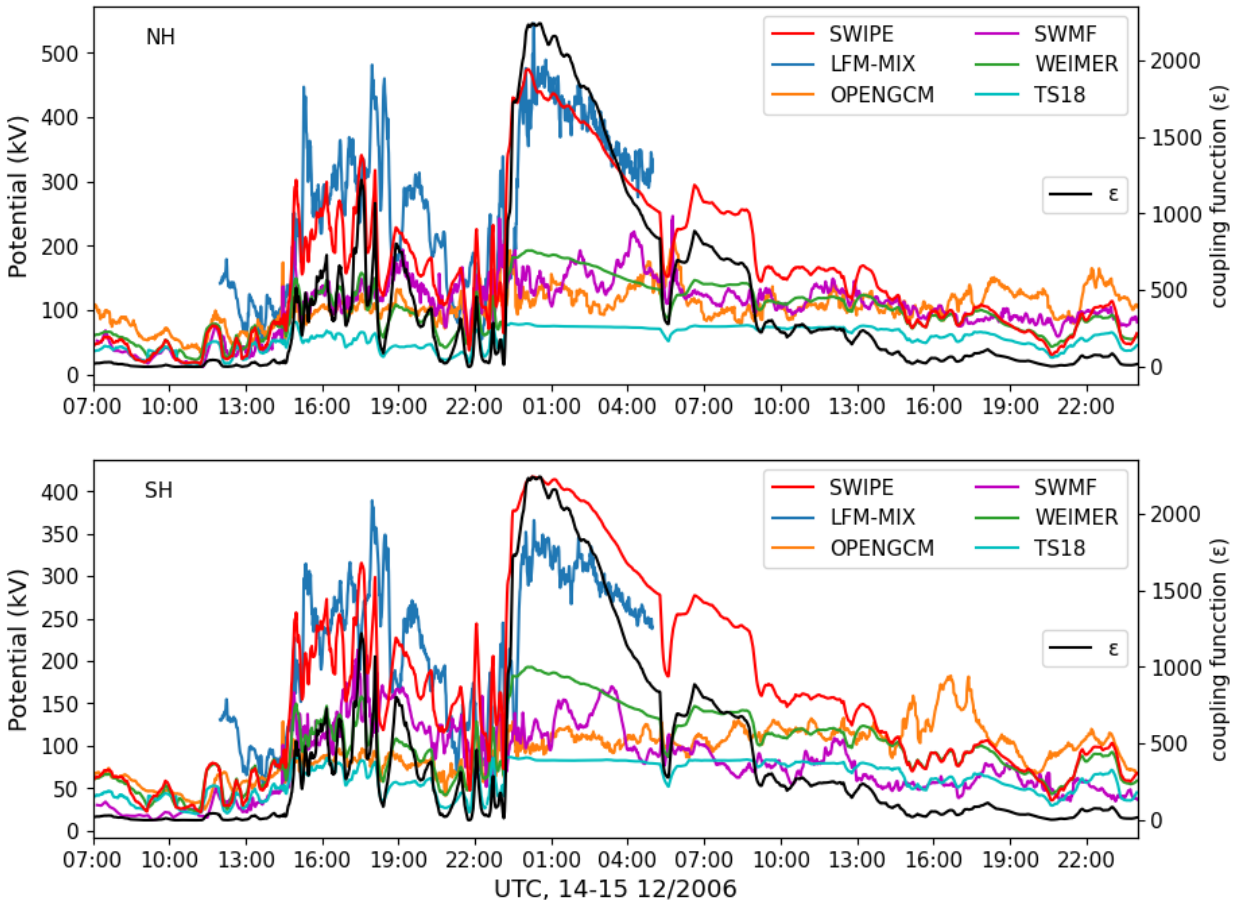

Figure 9: CPCP as time series from the selected models (colored lines) in the NH (top) and SH (bottom) with scale on the left side. Also included is the Newell coupling function (ϵ, scale on the right).

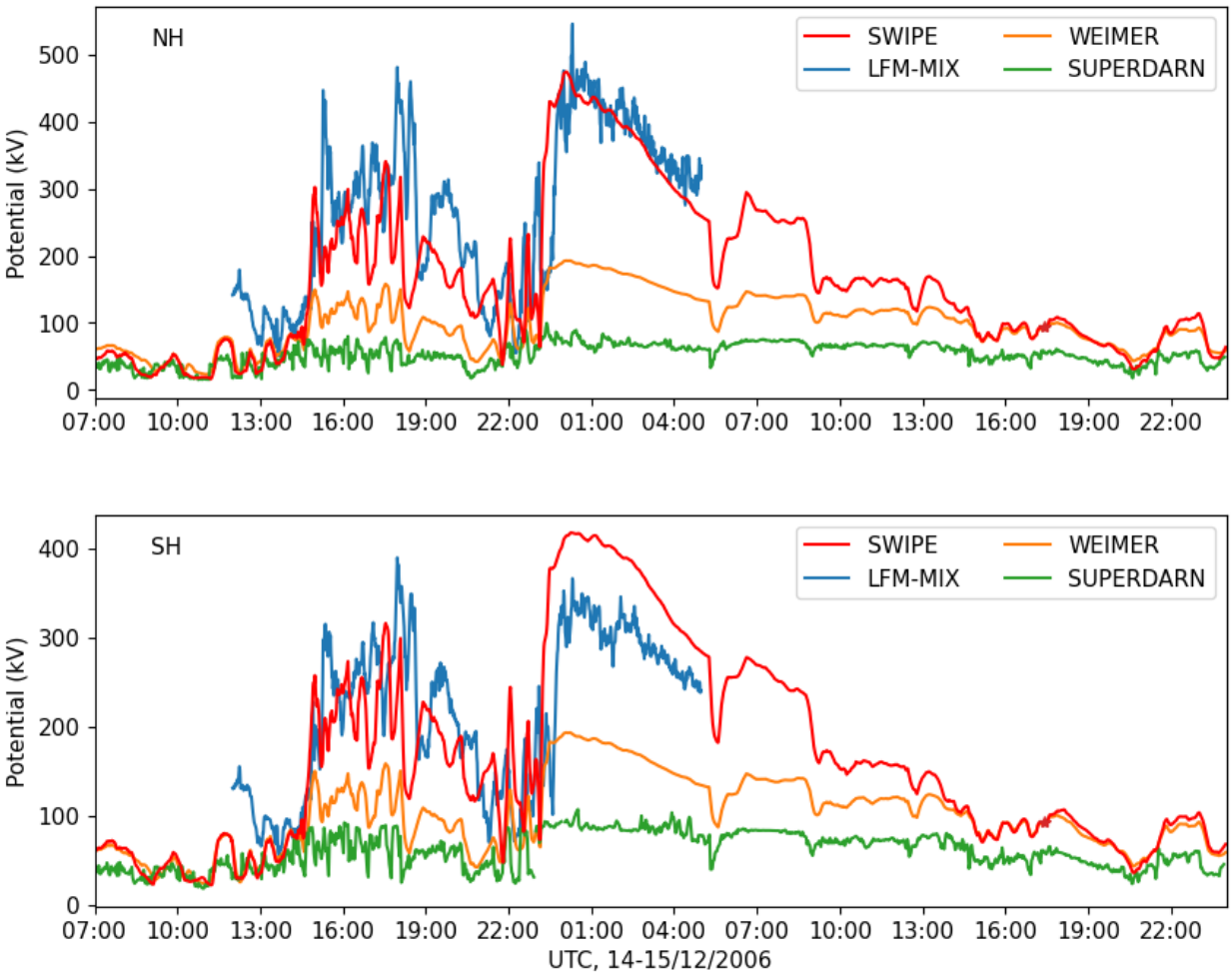

Figure 10: Same as Figure 9, but for clarity showing only selected models without the Newel coupling function. The CPCP from SuperDARN data product is added.

4 Electromagnetic work (Joule heating) and Poynting flux

In this Section we compare the electromagnetic work and Poynting flux produced by the Hi-C (or SWIPE) model to the other models listed in Section 2.2 in the storm event described in Section 2.1. The approach is nearly identical to the one used in Section 3 for the electrostatic potential.

4.1 Electromagnetic work

Figure 11 presents the Mlat-MLT distributions of the electrostatic work in the NH (upper part) and SH (lower par) for the moderate activity case from SWIPE and the models available at CCMC (listed in Table 2). It should be noted that this is not necessarily identical to the Joule heating, as discussed by Hatch et al. [2023]. Also in this case the two statistical models, SWIPE and Weimer, arguably show the greatest similarity between any two models, although also the SWMF result is rather similar to the statistical models. Otherwise the variability between the models is large, both in spatial distribution and in magnitude. It is interesting to note that some of the models produce rather large electromagnetic work in the polar cap, while in others it is concentrated in the vicinity of the auroral oval. While each model shows some hemispheric differences, it may be said that the hemispheric difference for each model are smaller than the differences between the models.

Figure 12 shows the electromagnetic work from selected models for the three different activity levels marked in Figure 5. As was the case with the potential and CPCP discussed in Section 3, also in the electromagnetic work SWIPE shows much stronger response to the solar wind driving than the Weimer or SWMF models. In SWIPE the hemispherically integrated electromagnetic work increases by a factor of 57 from the quiet to the active conditions, while for Weimer and SWMF the factor is 12 and 27, respectively. In contrast, SWIPE shows the smallest change in the spatial extent of the electromagnetic work. While the SWMF and especially the Weimer model show a marked equatorward expansion, the region of maximum electromagnetic work predicted by SWIPE moves only a few degrees southward.

Figure 13 shows time series of the hemispherically integrated electromagnetic work from different models for the NH and SH, together with the Newell coupling function. Note that time series data was not available from all the models used in the previous figures. The models in Figure 13 show large spread in values during the extreme solar wind driving, first starting with the very large solar wind speed at around 14 UT on December 14 and then intensifying with the strongly negative IMF Bz around 0 UT on December 15. Apart from the OpenCGM model, differences between the models seem to be smaller in the SH than NH, especially in the recovery phase. Similarly to the CPCP discussed in Section 3, the electromagnetic work predicted by SWIPE seems to be closely correlated with the coupling function during the extreme driving. This seemingly linear correlation is somewhat surprising, given that the electromagnetic work could be expected to scale as electric field squared.

4.2 Poynting flux

It is a very common assumption to equate the ionospheric Joule heating (or in fact the electromagnetic work) and the Poynting flux flowing from the magnetosphere to the ionosphere. For references, examples and discussion of the validity of this assumption, we refer to Richmond [2010] and Vanhamäki et al. [2012]. In the modeling challenge described by Rastätter et al. [2016] this assumption was used almost exclusively, so the actual Poynting flux is not generally available. Here

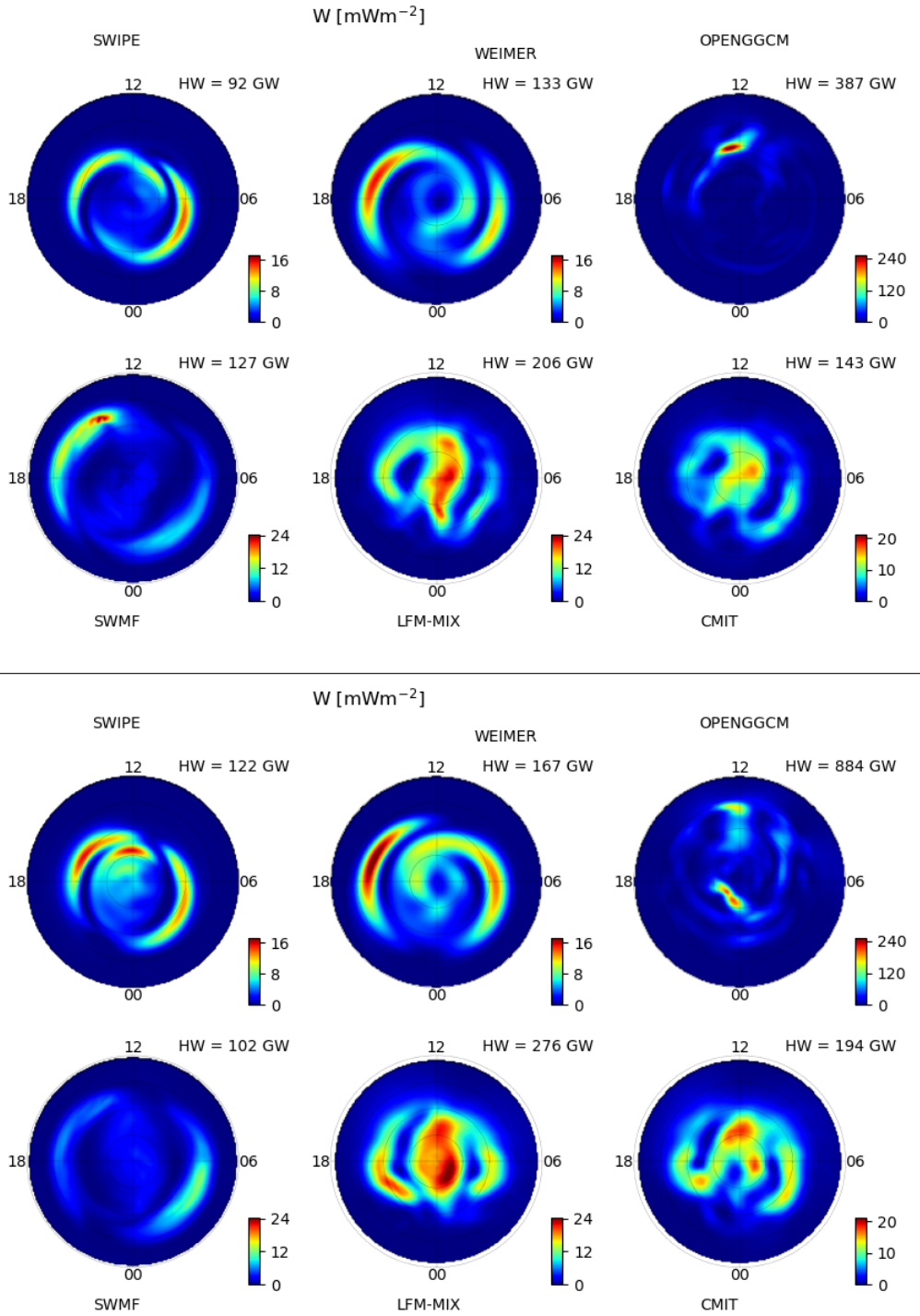

Figure 11: Electromagnetic work from SWIPE and models from CCMC for the moderate conditions described in Figure 5 and Table 1. NH at top, SH at bottom. Corresponds to the electrostatic potential shown in Figure 6. Note the different color scales.

we present comparison between the SWIPE and Cosgrove model (see Table 2) for the Poynting flux, and at the same time check how closely the electromagnetic work and Poynting flux given by

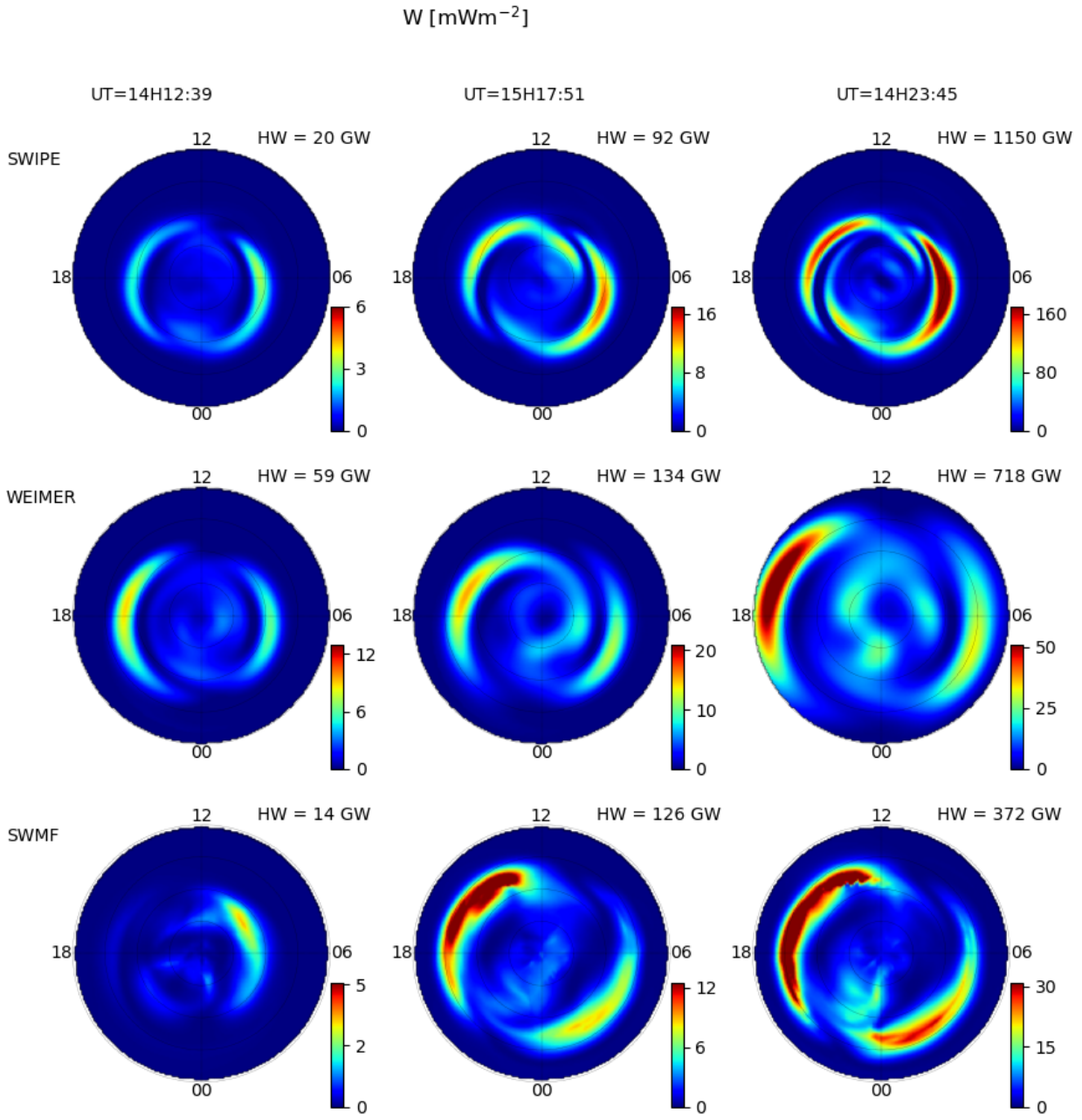

Figure 12: Electromagnetic work at NH from SWIPE (top row), Weimer-05 (middle row) and SWMF (bottom row) at the three selected times indicated in Figure: left 15-Dec 21:07 UT (quiet conditions), middle 14-Dec 14:50 UT (moderate) and right 14-Dec 23:45 UT (active). Corresponds to the electrostatic potential shown in Figure 8. Note the different color scales.

the SWIPE model match each other.

Figure 14 shows the electromagnetic work from SWIPE (same as in Figure 12) together with the Poynting flux from the SWIPE and Cosgrove models in the NH for the three different activity levels marked in Figure 5. It is obvious that the electromagnetic work and Poynting flux given by

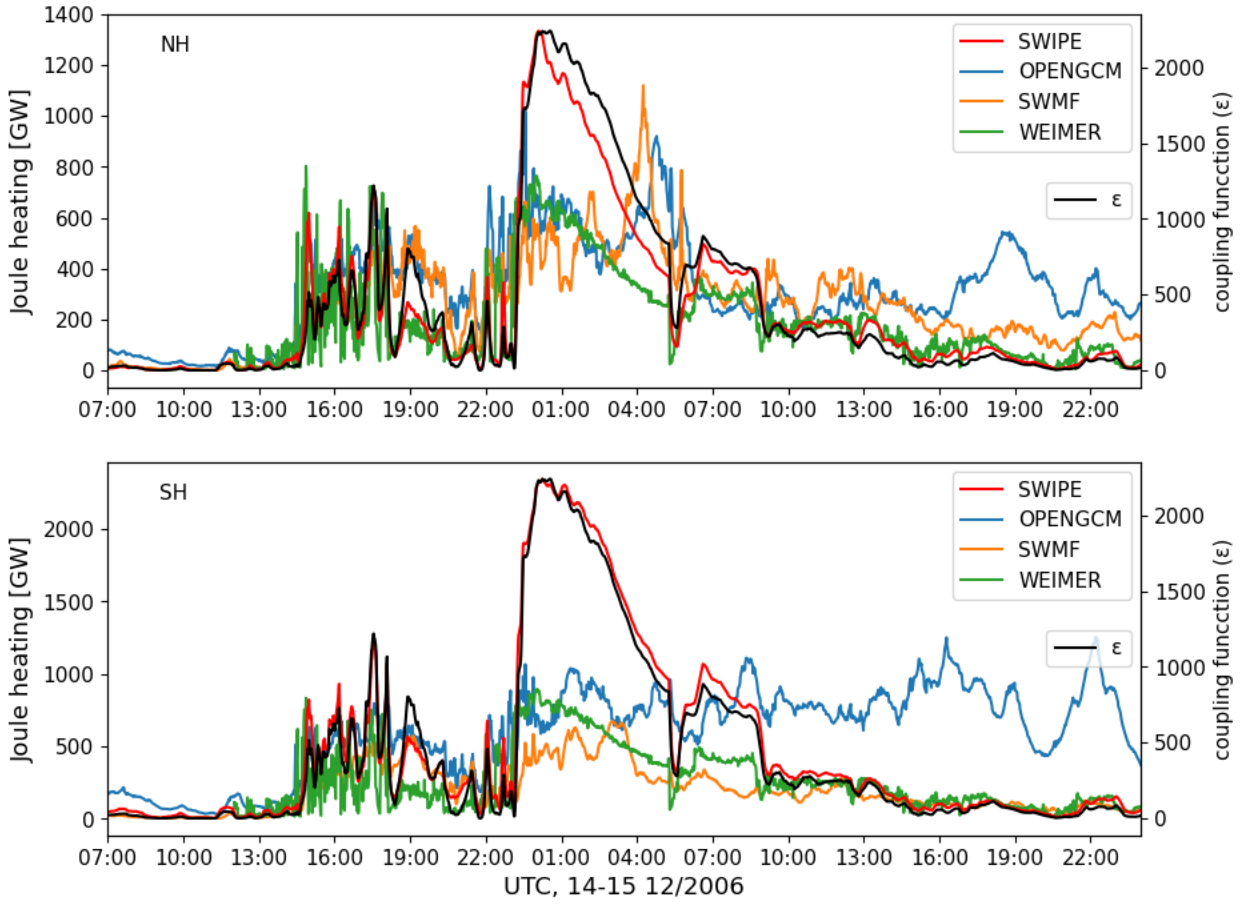

Figure 13: Hemispherically integrated electromagnetic work as time series from the selected models (colored lines) in the NH (top) and SH (bottom) with scale on the left side. Also included is the Newel coupling function (ϵ, scale on the right). Corresponds to the electrostatic potential shown in Figure 9. Note the different scales for the two hemispheres.

SWIPE are very closely matched, although not quite identical. An exact match is not expected, as discussed by Richmond [2010] and Vanhamäki et al. [2012], but the close resemblance is an indication that the model has been constructed in a self-consistent manner. A similar result is seen also in the SH (plot not shown). It is interesting to note that the Cosgrove Poynting flux model gives nearly identical spatial pattern for the three activity levels, which very different behaviour from the electromagnetic work given by the SWIPE, Weimer and SWMF models in Figure 12.

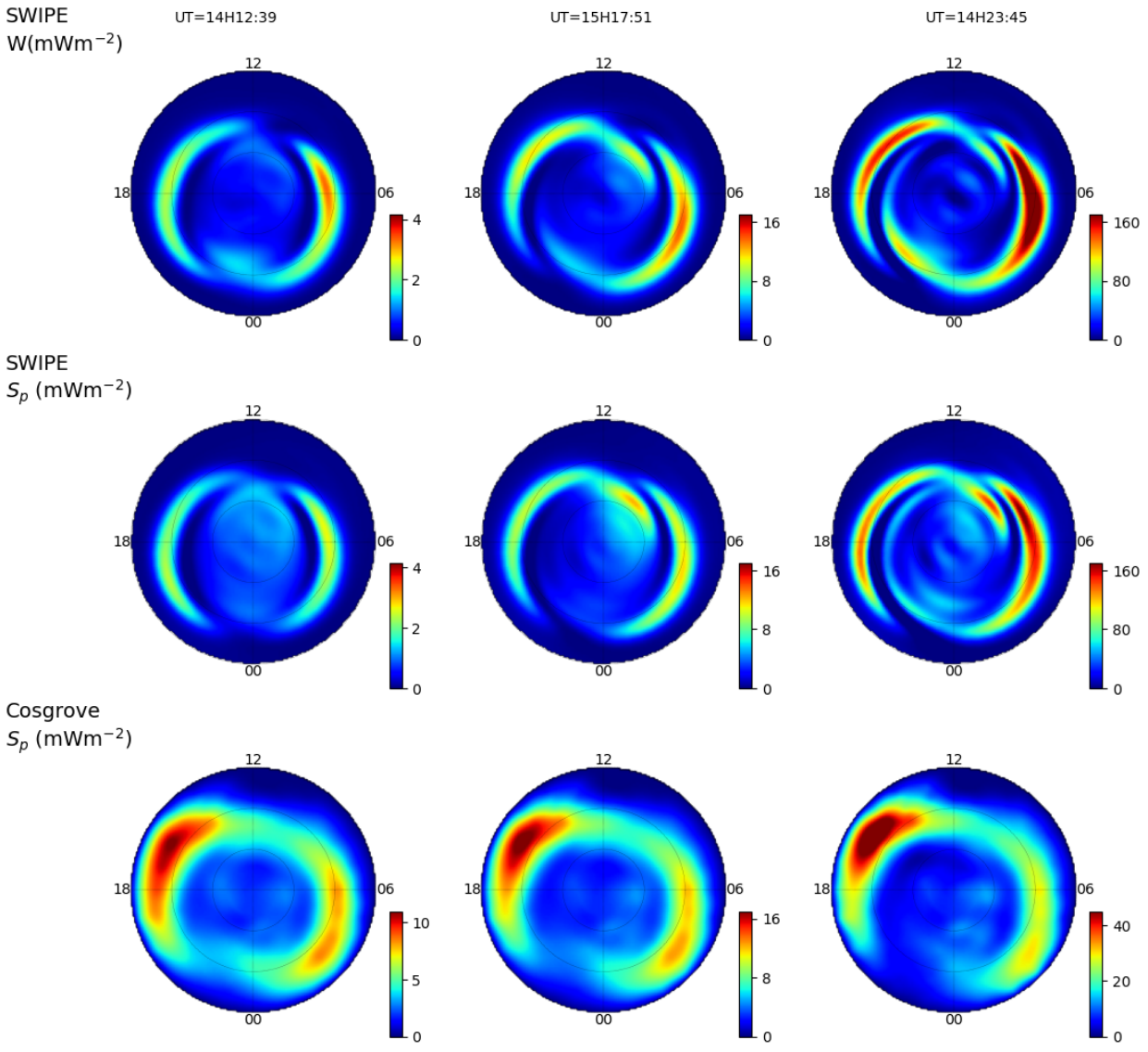

Figure 14: Electromagnetic work from SWIPE (top row) together with the Poynting flux from SWIPE (middle row) and from Cosgrove model in the NH at the three selected times indicated in Figure: left 15-Dec 21:07 UT (quiet conditions), middle 14-Dec 14:50 UT (moderate) and right 14-Dec 23:45 UT (active). The top row is the same as in Figure 12. Note the different color scales.

5 Conductances

In this Section we first compare the Pedersen and Hall conductances produced by the Hi-C (or SWIPE) model to the other models listed in Section 2.2 in the storm event described in Section 2.1. The approach is nearly identical to the one used in Section 3 for the electrostatic potential and in Section 4 for the electromagnetic work. In addition, we also present a comparison of Pedersen conductances produced by SWIPE with those calculated from the same Swarm dataset using the method by Sugiura et al. [1982].

5.1 Pedersen and Hall conductances during the GEM-CEDAR storm

As the Hall and Pedersen conductances behave in a very similar manner in the examples shown by Hatch et al. [2023], we concentrate here mostly on the Pedersen conductance.

Figure 15 presents the Mlat-MLT distributions of the Pedersen conductance in the NH (upper part) and SH (lower par) for the moderate activity case from SWIPE and the models available at CCMC (listed in Table 2). It should be noted that here the Weimer model has been replaced by the Hardy model [Hardy et al., 1987] calculated using code available in the Lompe GitHub repository, as the Weimer model does not include conductances. Also in this case the various models show large range of variability, both in magnitude and in spatial distribution. Here, in contrast to the electrostatic potential and electromagnetic work, it can not be said that the statistical models would be closer to each other than to the simulations. In general the conductances are weaker in the NH than in the south, which can be expected as the storm takes place in December.

One striking feature in Figure 15 is the variability in the ratio of day-side and nighttime oval conductances. SWIPE does not produce practically any day-side enhancements, while the oval conductances are clearly elevated. SWFM behaves in somewhat similar manner, but does show some day-side enhancements. LFM-Mix and CMIT represent the other extreme, where the day-side solar induced enhancement is clear, but the oval is very weak or invisible. Hardy shows both the oval and day-side solar background clearly, while in OpenCGM even the day-side seems to be dominated by the oval.

Figure 16 shows the Hall conductance in the same manner and for the same conditions as for the Pedersen conductance shown in the previous figure. In all the models the general patterns are the same for the two conductances. However, the Hall conductance is typically larger and in many of the models the nightside oval is more clearly visible in the Hall conductance. Also in this case the variability between the modes is striking.

Figure 17 shows the NH Pedersen conductance from selected models for the three different activity levels marked in Figure 5. It seems that the Pedersen conductance in SWIPE remains more or less at the same level during all the three activity conditions. Especially in the morning sector the variability is small, but in the evening and noon sectors the conductance does get bit larger as the geomagnetic activity level increases. However, these enhancements are small when compared to the Hardy and SWFM models, which show large increase in the magnitude of the Pedersen conductance and clear expansion of the oval to lower latitudes.

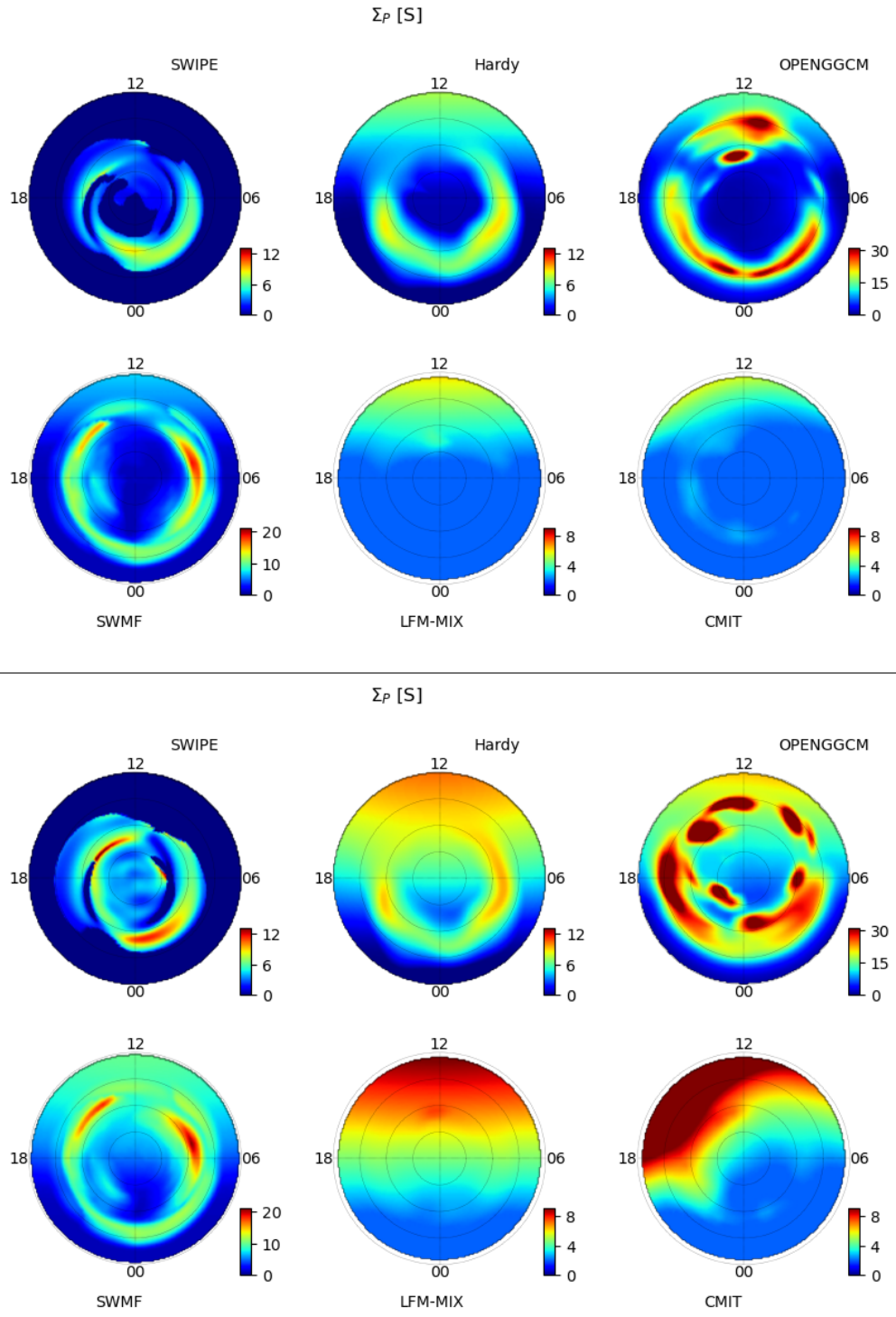

Figure 15: Pedersen conductance from SWIPE and models from CCMC for the moderate conditions described in Figure 5 and Table 1. NH at top, SH at bottom. Corresponds to the electric potential shown in Figure 6 and electromagnetic work in Figure 11, except Hardy model replaces the Weimer-05 model. Note the different color scales.

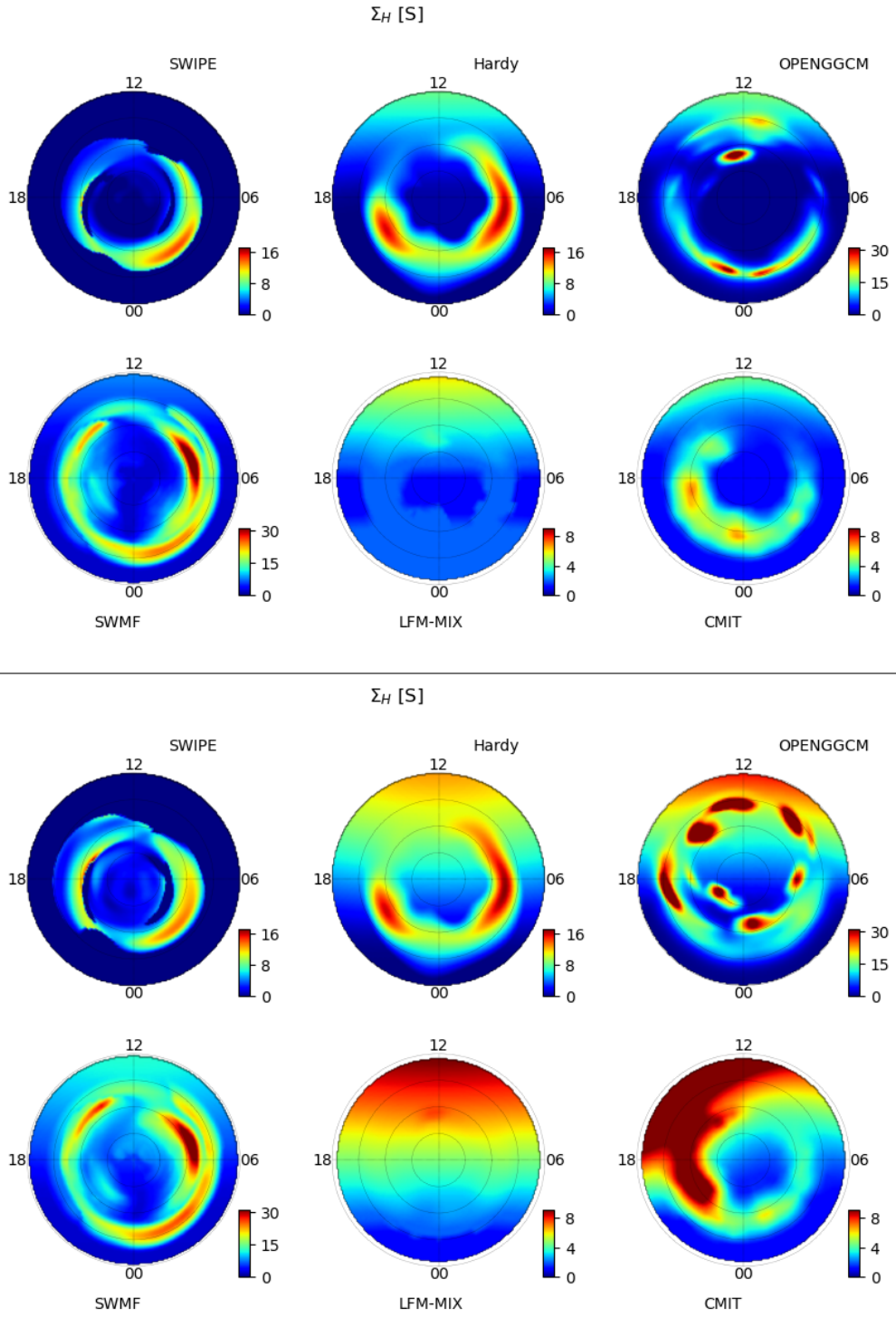

Figure 16: Same as Figure 15, but for the Hall conductance. Note the different color scales.

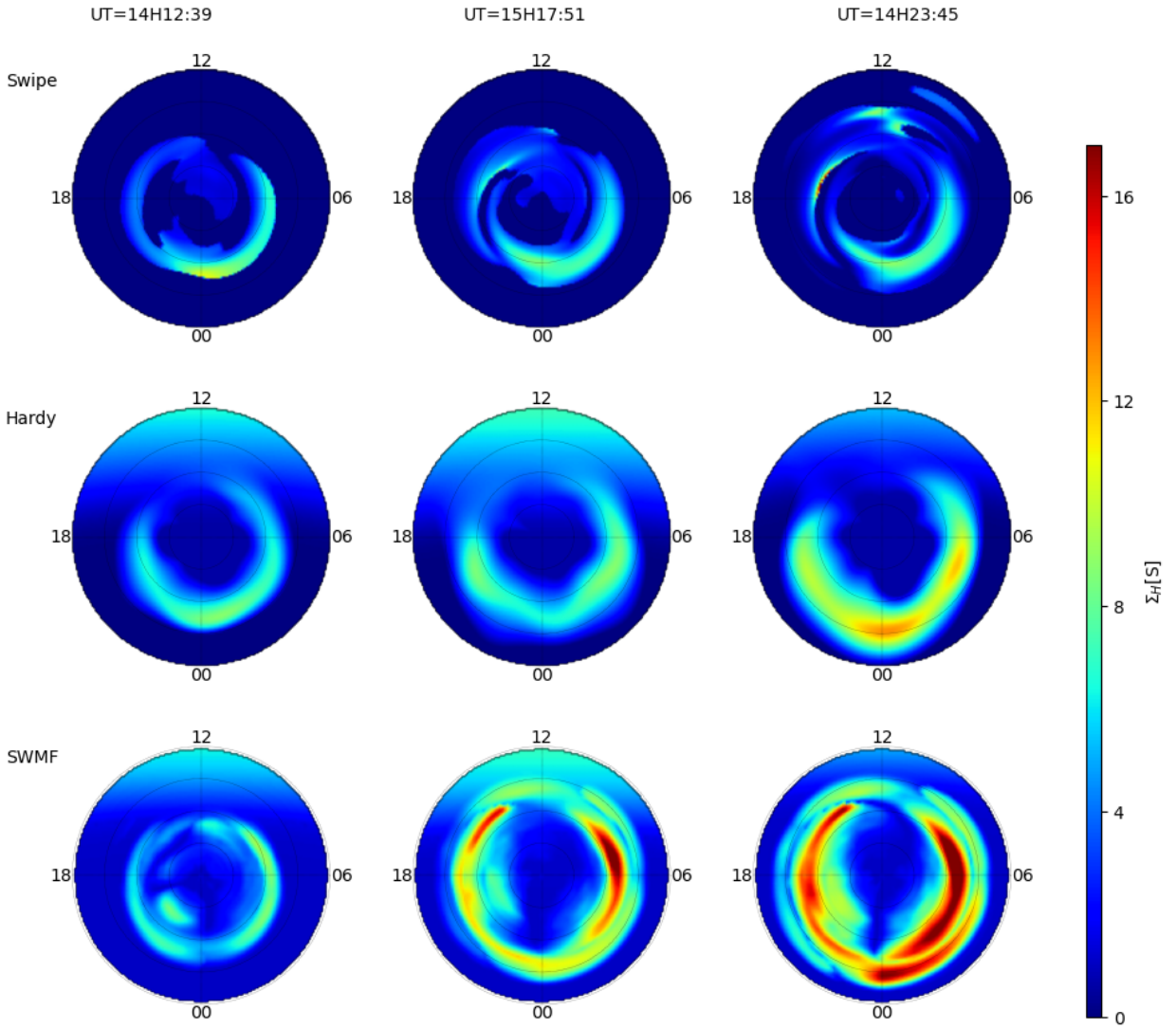

Figure 17: Pedersen conductance at NH from SWIPE (top row), Hardy (middle row) and SWMF (bottom row) at the three selected times indicated in Figure 5: left 15-Dec 21:07 UT (moderate activity), middle 14-Dec 14:50 UT (high activity) and right 14-Dec 23:45 UT (extreme activity). Corresponds to the electric potential shown in Figure 8 electromagnetic work in Figure 12, except Hardy model replaces the Weimer-05 model.

5.2 Comparison of Swarm-based Pedersen conductance estimates

Figure 18 presents a comparison between two statistical Pedersen conductance estimates calculated in different ways. On the left is the SWIPE estimate, which is based on first creating global parametrized models of the currents (the AMPS model) and the convection (the Hi-C model) and putting them together as described in Hatch et al. [2023]. On the right is a model based on the analysis method developed by Sugiura et al. [1982], where the Pedersen conductance is estimated from individual measurements of the electric and magnetic fields by the Swarm-A and -B satellites.

The method by Sugiura et al. [1982] has been applied to the Swarm data by Juusola et al. [2016] and Vanhamäki et al. [2021]. In this work the analysis was extended to cover all available Swarm-A and -B data from December 2013 to April 2023. A short summary of the analysis steps is as follows.

- Only cross-track (ct) ion velocity $V_{ion,ct}$ is used and data with bad calibrations flags is removed.
- CHAOS-7 model [Finlay et al., 2020] is removed from the measured magnetic field and the cross-track disturbance ΔB_{ct} is calculated.
- Both $V_{ion,ct}$ and ΔB_{ct} are smoothed with a 13 point moving median (about 45 km for the 2 Hz data).
- A slope is fitted between the $V_{ion,ct}$ and ΔB_{ct} data using 13 point moving window. Also the correlation coefficient between the $V_{ion,ct}$ and ΔB_{ct} data is calculated in the same window.
- The slope gives the Pedersen conductance for these data points, but the estimate is accepted only if the correlation coefficient is smaller than -0.7.

This procedure is repeated for all the available data. The obtained Pedersen conductances corresponding to the selected solar wind and IMF conditions are binned to MLT-MLAT grid and the median in each grid cell is shown in Figure 18.

As the selected GEM-CEDAR storm has very large solar wind speed during the whole event, it was not possible to get meaningful statistics with the Sugiura et al. [1982] method even for the "quiet" condition. In stead, in Figure 18 shows comparisons during more typical conditions.

In all the cases shown in Figure 18 the SWIPE model uses solar wind speed 400 km/s, dipole tilt 0° and F10.7=120, while the IMZ y- and z-components get values of 0 or ±2, as indicated in the figure. To get enough statistics, the Sugiura estimate shows median of data points with speed in the range of 300-500 km/s and the IMF components in 4 nT wide range around the central point (e.g. between 0-4 nT when SWIPE uses 2 nT).

The limited region where the SWIPE estimate is valid makes comparisons difficult. Nevertheless, it is clear that both methods give similar magnitudes for the Pedersen conductance. Also the differences between the morning and evening sectors are similar, as is the day-night difference in the bottom row. Furthermore, both methods seem to give an afternoon conductance enhancement at high latitudes. It is also interesting to note that the Sugiura result does not show any clear dayside enhancement due to solar photo-ionization.

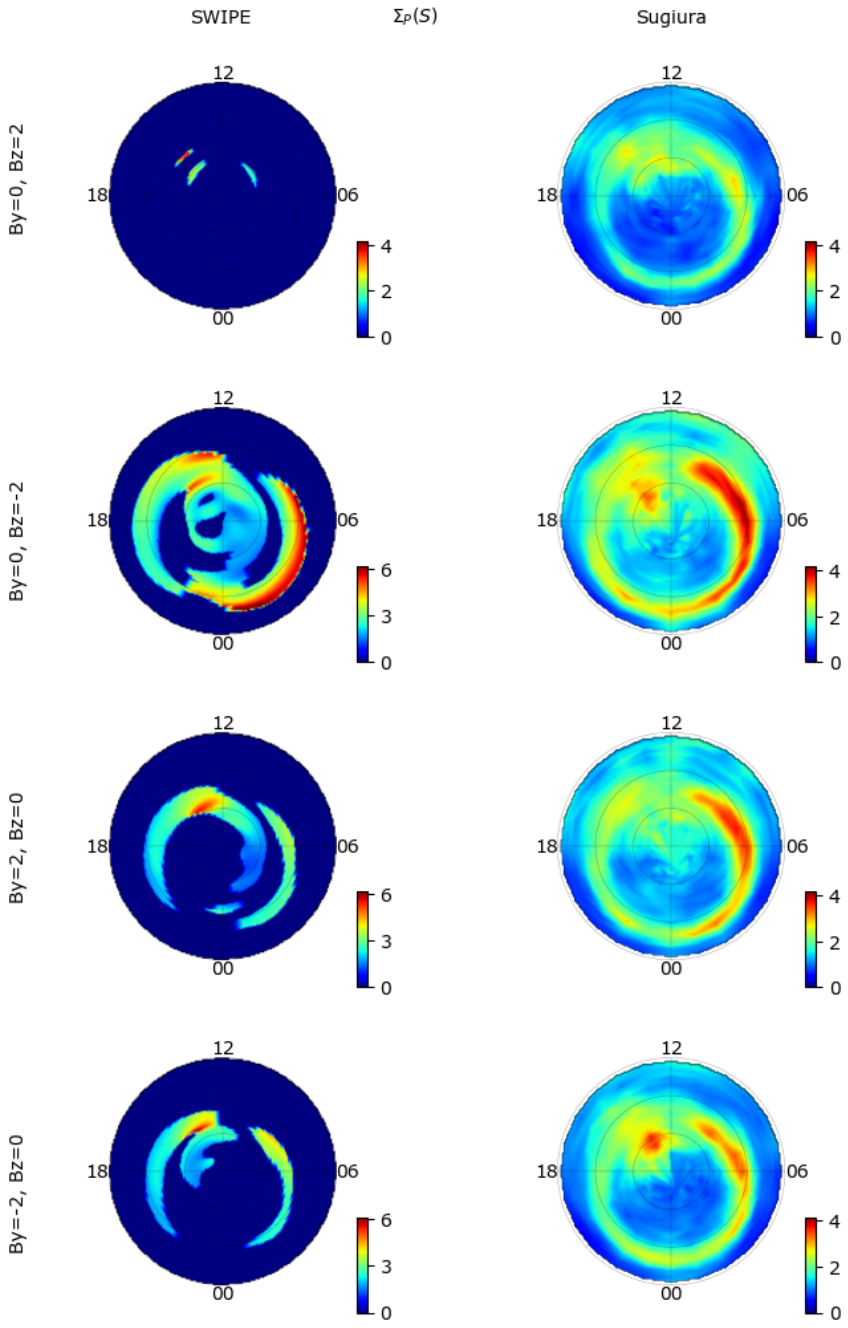

Figure 18: Pedersen conductance from the SWIPE model (left column) and directly from the Swarm data with the analysis method by Sugiura et al. [1982] (right column) for different IMF conditions (rows). In SWIPE calculation the solar wind speed is 400 km/s, dipole tilt is 0° and F10.7=120. See text for more details. Note the different color scales.

6 Summary

In this report we have presented validation efforts of the Swarm High-latitude Convection (Swarm Hi-C) model that has been developed in the Swarm Ionospheric Polar Electrodynamics (SWIPE) project and is published in the article Hatch et al. [2023]. In synthetic events where either the solar wind speed or the IMF B_z changes while other input parameters remain fixed, the model behaves in a consistent and expected manner. In the 14-16 December 2006 storm, used as a part of the GEM-CEDAR modeling challenge, the SWIPE model did produce results that are comparable to the other evaluated models. Following points can be noted:

- The selected storm contained periods when the solar wind driving was extreme, pushing the models to uncharted territory.
- During low and moderate solar wind driving, SWIPE predictions of the electrostatic potential, CPCP and electromagnetic work were close to the statistical Weimer model.
- During extreme solar driving the electrostatic potential, CPCP and electromagnetic work predicted by SWIPE scale almost linearly with the Newell coupling function. This is in contrast to many other models, but resembles behavior of the LFM-Mix simulation.
- The Pedersen conductance predicted by SWIPE, in contrast to the potential and electromagnetic work, does not seem to react strongly to the solar wind driving.
- Variations in the latitudinal extent of the oval seem to be smaller in SWIPE than in most of the other models.
- In all the studied output parameters (i.e. the potential, electromagnetic work and Pedersen conductance) the variability between the various models is surprisingly large, both in spatial distribution and in magnitude.

The last point highlight the continued need to improve modeling of the high-latitude ionospheric electrodynamics.

References

[URL1]: GEM-CEDAR challenge at CCMC https://ccmc.gsfc.nasa.gov/challenges/gem-cedar/

[URL2]: OMNIweb database https://omniweb.gsfc.nasa.gov/

[URL3]: SWMF simulation run for the GEM-CEDAR challenge
https://ccmc.gsfc.nasa.gov/results/viewrun.php?domain=GM&runnumber=SWPC_SWMF_052811_2

[URL4]: Weimer model run for the GEM-CEDAR challenge
https://ccmc.gsfc.nasa.gov/results/viewrun.php?domain=IT&runnumber=PF_WEIMER_021515_IT_2

[URL5]: OpenCGM simulation run for the GEM-CEDAR challenge
https://ccmc.gsfc.nasa.gov/results/viewrun.php?domain=GM&runnumber=SWPC_OpenGGCM_031111_2

[URL6]: LFM-MIX simulation run for the GEM-CEDAR challenge
https://ccmc.gsfc.nasa.gov/results/viewrun.php?domain=GM&runnumber=SWPC_CMIT-LFM-MIX_031711_2

[URL7]: CMIT simulation run for the GEM-CEDAR challenge https://ccmc.gsfc.nasa.gov/results/viewrun.php?domain=GM&runnumber=SWPC_CMIT-LFM-MIX-TIEGCM_031711_2

[URL8]: SuperDARN http://vt.superdarn.org/

Finlay C.C., C. Kloss, N. Olsen, M. Hammer, L. Toeffner-Clausen, A. Grayver, and A. Kuvshinov: The CHAOS-7 geomagnetic field model and observed changes in the South Atlantic Anomaly. *Earth Planets Space*, 72, doi:10.1186/s40623-020-01252-9, 2020.

Hardy D.A., M.S. Gussenhoven, R. Raistrick, and W.J. McNeil: Statistical and functional representations of the pattern of auroral energy flux, number flux, and conductivity. *J. Geophys. Res.*, 92 (A11), 12275–12294, doi:10.1029/JA092iA11p12275, 1987.

Hatch S. M., H. Vanhamäki, J. K. Burchill, D. J. Knudsen, K. M. Laundal, L. Lomidze, M. Madelaire, J. P. Reistad: Does high-latitude ionospheric electrodynamics exhibit hemispheric mirror symmetry? *submitted to Annales Geophysicae*, https://doi.org/10.5194/egusphere-2023-2920 2024.

Juusola L., W. Archer, K. Kauristie, H. Vanhamäki, and A. Aikio: Ionospheric Conductances of a Morning-Sector Auroral Arc From Swarm Measurements, *Geophys. Res. Lett.*, 43, 11519–11527, doi:10.1002/2016GL070248, 2016.

Newell P.T., T. Sotirelis, K. Liou, C.-I. Meng, and F. J. Rich: A nearly universal solar wind-magnetosphere coupling function inferred from 10 magnetospheric state variables. *J. Geophys. Res.*, 112, A01206, doi:10.1029/2006JA012015, 2007.

Thomas E.G., and S.G. Shepherd: Statistical patterns of ionospheric convection derived from mid-latitude, high-latitude, and polar SuperDARN HF radar observations. *J. Geophys. Res*, 123, 3196-3216 doi:10.1002/2018JA025280, 2018.

Rastätter L., J. S. Shim, M. M. Kuznetsova, et al.: GEM-CEDAR challenge: Poynting flux at DMSP and modeled Joule heat. *Space Weather*, 14, 113–135, doi:10.1002/2015SW001238, 2016.

Richmond A.D.: On the ionospheric application of Poynting's theorem. *J. Geophys. Res.*, 115, doi:10.1029/2010JA015768, 2010.

Sugiura M., N.C. Maynard, W.H. Farthing, J.P. Heppner, B.G. Ledley, and L.J. Cahill: Initial results on the correlation between the magnetic and electric fields observed from the DE-2 satellite in the field-aligned current regions. *Geophys. Res. Lett.*, 9, 985–988, doi:10.1029/GL009i009p00985, 1982.

Vanhamäki H., A. Yoshikawa, O. Amm, and R. Fujii: Ionospheric Joule heating and Poynting flux in quasi-static approximation. *J. Geophys. Res.*, 117, doi:10.1029/2012JA017841, 2012.

Vanhamäki H., A. Aikio, K. Kauristie, S. Käki, and D. Knudsen: Statistical estimates of auroral Pedersen conductance using electric and magnetic measurements by the Swarm spacecraft. *EGU General Assembly 2021*, online, EGU21-12569, doi:10.5194/egusphere-egu21-12569, 2021.

Weimer, D. R., Improved ionospheric electrodynamic models and application to calculating Joule heating rates, Journal of Geophysical Research, 110, A05306, doi:10.1029/2004JA010884, 2005.

Cosgrove, R. B., Bahcivan, H., Chen, S., Strangeway, R. J., Ortega, J., Alhassan, M., et al., Empirical model of Poynting flux derived from FAST data and a cusp signature. Journal of Geophysical Research: Space Physics, 119(1), doi:10.1002/2013ja019105, 2014.